Published in final edited form as:
Channels (Austin). 2009 ; 3(1): 6–11.

Mitsugumin 53-mediated maintenance of K^+ currents in cardiac myocytes

Haruko Masumiya[1,2], **Yasuhide Asaumi**[3], **Miyuki Nishi**[1,4], **Susumu Minamisawa**[5], **Satomi Adachi-Akahane**[6], **Morikatsu Yoshida**[1,7], **Kenji Kangawa**[7], **Kenta Ito**[3], **Yutaka Kagaya**[3], **Teruyuki Yanagisawa**[2], **Tetsuo Yamazaki**[1,4], **Jianjie Ma**[8], and **Hiroshi Takeshima**[1,4,*]

[1] Department of Medical Chemistry, Tohoku University Graduate School of Medicine; Sendai, Japan

[2] Department of Molecular Pharmacology, Tohoku University Graduate School of Medicine; Sendai, Japan

[3] Department of Cardiovascular Medicine, Tohoku University Graduate School of Medicine; Sendai, Japan

[4] Department of Biochemistry, Kyoto University Graduate School of Pharmaceutical Sciences, Kyoto, Japan

[5] Department of Life Science and Medical Bioscience, Waseda University Graduate School of Advanced Science and Engineering, Tokyo, Japan

[6] Department of Pharmacology, Toho University School of Medicine, Tokyo, Japan

[7] Department of Biochemistry, National Cardiovascular Center Research Institute, Osaka, Japan

[8] Department of Physiology and Biophysics, Robert Wood Johnson Medical School, Piscataway, NJ USA

Abstract

Mitsugumin 53 (MG53) is a muscle-specific RBCC/TRIM family member predominantly localized on small vesicles underneath the plasma membrane. Upon cell-surface lesion MG53 recruits the vesicles to the repair site in an oxidation-dependent manner and MG53-knockout mice develop progressive myopathy associated with defective membrane repair. In this report, we focus on MG53-knockout cardiomyocytes showing abnormal action potential profile and a reduced K^+ current density. In cDNA expression experiments using cultured cells, $K_V2.1$-mediated currents were remarkably increased by MG53 without affecting the total and cell-surface levels of channel expression. In imaging analysis MG53 seemed to facilitate the mobility of $K_V2.1$-containing endocytic vesicles with acidic pH. However, similar effects on the current density and vesicular mobility were not observed in the putative dominant-negative form of MG53. Our data suggest that MG53 is involved in a constitutive cycle of certain cell-surface proteins between the plasma membrane and endosome-like vesicles in striated muscle, and also imply that the vesicular dynamics are essential for the quality control of $K_V2.1$ in cardiomyocytes.

[*]Correspondence to: Hiroshi Takeshima; Department of Biochemistry; Kyoto University Graduate School of Pharmaceutical Sciences; Kyoto 606-8501 Japan; Tel.: +81.75.753.4572; Fax: +81.75.753.4605; takeshim@pharm.kyoto-u.ac.jp.

NoteSupplementary materials can be found at: www.landesbioscience.com/supplement/MasumiyaCHAN3-1-Sup.pdf

Keywords

cardiac muscle; $K_V2.1$; RBCC/TRIM family; membrane recycling; membrane repair; mitsugumin 53; vesicular trafficking

Introduction

The RBCC/TRIM family proteins share the highly conserved tripartite motif, composed of Ring finger, B-box and Coiled-coil domains, in their N-terminal regions.[1] Based on the composition of motifs in the C-terminal region, ~70 TRIM proteins deduced from mammalian genomes are classified to subgroups, making up groups C-I~IX (ref. [2]). Some TRIM proteins indeed function as ubiquitin E3 ligases, involved in cancerogenesis, morphogenesis and viral infection, and therefore several human diseases are linked to mutations of TRIM proteins.[3] However, no common biological function has been established in the TRIM family, and the physiological roles of the family members are largely unknown.

Mitsugumin 53 (MG53) has been identified as a muscle-specific TRIM family protein from our immunoproteomics library.[4] In addition to the tripartite motif, MG53 and ~20 other family members contain PRY and SPRY domains in the C-terminal regions, and thus belong to the group C-IV.[2] MG53 is specifically expressed in skeletal and cardiac muscle, and is predominantly localized on intra-cellular vesicles underneath the cell membrane. In MG53-knockout mice showing a progressive muscular dystrophy-like phenotype, the mutant muscle is associated with defective membrane-repair capacity following damage to the cell surface. During membrane repair, MG53-containing vesicles are recruited to the injury sites for membrane-patch formation, and MG53 seems to trigger vesicle translocation by sensing the extracellular oxidative environment.[5] Moreover, our cDNA expression study in cultured cells also demonstrated that MG53 interacts with caveolin-3 to enhance vesicle transport to and budding from the cell membrane, suggesting the contribution of MG53 to steady state muscle membrane trafficking.[6] Here we report the data suggesting that MG53-mediated membrane trafficking maintains cell-surface K^+ current density to assure the integrity of the action potential profile in cardiomyocytes.

Results

Abnormal action potential profile in MG53-knockout cardio-myocytes

MG53-knockout mice with progressive myopathy showed a severely impaired running performance in our treadmill task.[5] Because MG53 is expressed in both skeletal and cardiac muscle cells, the deteriorated performance may suggest functional impairments of the heart as well as limb muscle. For characterizing the juvenile heart defects of MG53-knockout mice (8–12 week old), we first utilized electrocardiography. The monitoring detected complete atrioven-tricular block on rare occasions in MG53-knockou mice (Fig. 1A). This defect likely reflects deficient membrane repair, increased cell death and cellular disconnection of the atrioventricular conduction system in mutant mice. However, mutant mice exhibited apparently normal parameters in hemodynamic and echocardiographic studies (data not shown). These in vivo examinations suggest that overall heart performance is apparently normal under resting conditions in MG53-knockout mice.

To survey defects at the cellular level, single cardiomyocytes were prepared from MG53-knockout mice. In amphotericin B-perforated patch recording, the mutant cardiomyocytes showed aberrant values in parameters depicting the action potential profile (Table 1), and the loss of MG53 especially distorted potential transition after the overshoot under basal

conditions (Fig. 1B). Moreover, the traces obtained before and after isopretenol application of β-adrenergic stimulation crossed each other in MG53-knockout myocytes. Such irregular crossing was never observed in control cardiomyocytes. In cell shortening and Ca^{2+} transient measurements, MG53-knockout cardiomyocytes exhibited normal responses under control conditions, but impaired performance when treated with the β-adrenergic agonist (Table 2). The observations clearly indicate certain electro-physiological abnormalities in MG53-knockout cardiomyocytes.

Weak delayed rectifier K^+ currents in MG53KO cardiomyocytes

Based on the damaged late phase in the action potential configuration, we can expect abnormal Ca^{2+} and/or K^+ currents in MG53-knockout cardiomyocytes. Therefore, L-type Ca^{2+} channel activity was examined with depolarizing voltage-clamp steps of 400 ms in the testing range between −50 and +40 mV from a holding potential of −50 mV. We detected no significant difference in the current density and voltage dependency of basal L-type Ca^{2+} channels between mutant and wild-type myocytes (Fig. 2A). Next, voltage-gated K^+ currents were recorded with voltage-clamp pulses of 400 ms in the range between −100 and +40 mV from a holding potential of −40 mV. The peak current densities at −10 to +40 mV in MG53-knockout myocytes were significantly smaller than those of wild-type myocytes (Fig. 2B), suggesting that delayed rectifier K^+ currents, designated *I*kr, were impaired in the mutant myocytes. The transient outward K^+ currents, named *I*to, were also examined with 400 ms depolarization pulses at +40 mV from a holding potential of −80 mV in the presence and absence of 4-amin-opyridine (4AP) as an *I*to inhibitor (Fig. 2C). MG53-knockout myocytes retained apparently normal 4AP-sensitive currents, but showed significantly impaired 4AP-insensitive currents. Moreover, we observed that tetraethylammonium chloride (TEA)-sensitive *I*kr currents in MG53-knockout myocytes were smaller than controls (data not shown). These results indicate that the loss of MG53 specifically reduces 4AP-insensitive and TEA-sensitive *I*kr currents in cardiac myocytes. Of several voltage-gated K^+ channel subtypes expressed in mouse cardiomyocytes,[7] $K_V2.1$ and HERG channels fit the category and thus might be inactivated in MG53-knockout myocytes.

Stimulation of $K_V2.1$-mediated K^+ currents by MG53

For the coexpression of $K_V2.1$ and MG53 by a single transcript in cultured cells, we constructed an expression plasmid, in which both cDNAs are linked by an internal ribosomal entry site element (Fig. 3). Voltage-gated K^+ currents in human embryonic kidney (HEK) cells coexpressing $K_V2.1$ and MG53 were significantly higher than those of control cells coexpressing $K_V2.1$ and EGFP. In contrast, $^+$ currents were remarkably diminished in the $K_V2.1$-mediated K cells coexpressing MG53-Ring(−), a mutant MG53 lacking positive contribution to membrane repair and vesicular trafficking in skeletal muscle.[5,6] On the other hand, these effects of MG53 and MG53-Ring(−) were not seen in $K_V1.2$ and $K_V3.1$. The results demonstrate that $K_V2.1$ channel activity is specifically facilitated by proposed MG53-mediated reactions, and that MG53-Ring(−) functions as a dominant negative form in the proposed reactions. However, no significant changes in $K_V2.1$ channel properties, including gating kinetics, voltage dependency and closing kinetics, were detected between MG53- and MG53-Ring(−)-expressing cells.

As described above, HERG channels may be also affected by MG53. We tried to examine HERG channel activity in similar cDNA expression study, but the transfected cells have wide fluctuations in current density and we could not evaluate the MG53 effect on HERG channels.

No effect of MG53 on $K_V2.1$ protein level

The transfected HEK cells were subjected to western blot analysis to examine protein levels of $K_V2.1$ (Fig. 4A). Total cellular $K_V2.1$ levels were indistinguishable between MG53- and MG53-Ring(−)-expressing cells. To examine cell-surface $K_V2.1$ levels, cell-surface proteins were biotinylated, solubilized with SDS, recovered with streptavidin-beads and analyzed by western blotting. Again, we detected no obvious difference in cell-surface expression of $K_V2.1$ between the cells (Fig. 4B). Therefore, MG53 seems to have no effect on protein stability or surface recruitment of $K_V2.1$. Based on the data on $K_V2.1$ currents enhanced by MG53 (Fig. 3), the blot experiments suggest that the protein qualities of cell-surface $^{+}$-conducting channel are $K_V2.1$ functioning as a K presumably different between MG53- and MG53-Ring(−)-expressing cells. In other words, the proposed MG53-mediated reactions likely increase the active population of cell-surface $K_V2.1$ proteins, while the proposed reactions can be remarkably interrupted by MG53-Ring(−).

MG53 enhances mobility of $K_V2.1$-containing endosomes

It is well known that many receptor proteins constitutively cycle between the plasma membrane and the endosome bearing acidic conditions. To survey intracellular trafficking of $K_V2.1$ around endosomes, HA-tagged $K_V2.1$ was surface-labeled with anti-HA antibody conjugated with the red-excited CypHer 5E dye,[8] which is non-fluorescent at neutral pH and becomes fluorescent at acidic pH. After labeling $K_V2.1$ with the dye on ice, the cells that were warmed immediately started to exhibit increased overall fluorescence intensity and produce fluorescent intracellular vesicles. Non-transfected cells did not show the fluorescent vesicles (data not shown), confirming that we can monitor the internalization of $K_V2.1$ with this imaging system. The increasing fluorescence profiles after surface labeling were similar between MG53- and MG53-Ring(−)-expressing cells, suggesting that MG53 has no obvious effects on $K_V2.1$ internalization (Fig. 4C).

In imaging analysis after sufficient labeling of $K_V2.1$ with the CypHer 5E dye, the cells coexpressing MG53 always contained small and active m in diameter) $K_V2.1$-bearing vesicles (0.2–0.5 μm in diameter) that moved around smoothly and occasionally disappeared quickly (Fig. 5A and Suppl. movie 1). However, the cells coexpressing MG53-Ring(−) predominantly contained small vesicles showing laggard movements (Fig. 5B and Suppl. movie 2). Statistical analysis showed that the mobility of the small vesicles in MG53-expressing cells was remarkably higher than that in MG53-Ring(−)-expressing cells (Fig. 5C). In both cells, large vesicles (1–2 μm in diameter) were always inactive. Therefore, MG53 seems to govern the mobility of small and acidic vesicles containing $K_V2.1$, possibly assigned as early and/or recycling endosomes.

Discussion

MG53-knockout cardiomyocytes showed impaired 4AP-insensitive *I* kr currents, where there are mainly mediated by $K_V2.1$ and HERG channels (Fig. 2). Our DNA expression study demonstrated that MG53 elevates $K_V2.1$-mediated current density and this effect was not observed in other channels examined (Fig. 3). Therefore, K_V $K_V2.1$-mediated currents are probably impaired in MG53-knockout cardiomyocytes. Based on the finding that the $K_V2.1$-mediated currents are stimulated by MG53 without affecting the channel properties and density (Figs. 3 and 4), we need to consider the molecular mechanism underlying the MG53-mediated channel activation. A previous study suggested that both cell-surface localization and phosphorylation of $K_V2.1$ are important determinants of its current density in neurons.[9] However, we could not detect band shift accompanied by $K_V2.1$ phosphorylation between the cells coexpressing MG53 and MG53-Ring(−) (Fig. 4), and protein phosphorylation does not regulate $K_V2.1$-mediated currents in this case. It is also

rather unlikely that MG53 acts as a specific binding partner for cell-surface $K_V2.1$ to stimulate its channel activity, for the following reasons: (i) our affinity-purification of MG53 did not suggest its direct interaction with $K_V2.1$, (ii) MG53 is predominantly localized on intracellular vesicles, and (iii) MG53 induces no changes in $K_V2.1$ channel kinetics. Therefore, it is still in mystery why MG53 activates $K_V2.1$-mediated currents.

MG53 is an essential component of the muscle membrane repair machinery.[5] Following cell-surface damage, MG53 probably senses an oxidized external environment for its oligomer formation, and mediates the nucleation of intracellular vesicles for patching injured cell membrane sites. Moreover, MG53 seems to take part in vesicular trafficking to and budding from the cell membrane in the steady state.[6] In this report, our imaging analysis demonstrates that $K_V2.1$ is in a constitutive cycle between the cell membrane and endosome-like vesicles when expressed in cultured cells (Fig. 4). Moreover, MG53 seemed to facilitate the mobility of $K_V2.1$-containing endosome-ike vesicles in a “Ring finger motif”-dependent manner (Fig. 5). Therefore, our data raise the possibility that the endosomal dynamics modulate the quality control of $K_V2.1$; for example, damaged $K_V2.1$ subunits could be repaired or replaced under acidic conditions in the endosome-like vesicles, or non-functional $K_V2.1$ channels could be efficiently sorted for lysosomal/proteosomal degradation in the endosome-like vesicles (Fig. 6). This proposed machinery is likely supported by caveolin-dependent endocytosis, because (i) MG53 does not affect the generation of clathrin-coated vesicles in amphibian embryonic cells, (ii) the effects of MG53 on vesicular trafficking are stimulated by coexpressing caveolin-3, and (iii) $K_V2.1$ proteins are predominantly localized on the membrane raft unrelated with the clathrin-mediated endocytosis when expressed in cultured cells.[6,10] Therefore, it is an attractive hypothesis that a set of certain cell-surface proteins including $K_V2.1$ may be functionally maintained by the predicted MG53-mediated quality control involving the endosome-like vesicle in striated muscle cells.

In addition to the hypothetical role in the quality control, we can propose that MG53-mediated vesicular trafficking may support the specific distribution of $K_V2.1$ to membrane rafts. Because cardiac $^{2+}$ ionic channels including $K_V2.1$, $K_V1.4$, $K_V1.5$ and the L-type Ca channels are known to localize in lipid rafts[11], the lipid environment might elevate the open probability of $K_V2.1$ channels. However, this proposal is unlikely for the following reasons. The raft disruption by depleting membrane cholesterol results in a marked voltage shift [12] while we detect in the steady-state inactivation of $K_V2.1$ channel, similar $K_V2.1$ channel kinetics between MG53- and MG53-Ring(−)- coexpressing cells (Fig. 3). MG53-knockout cardiomyocytes showed normal L-type Ca^{2+} channel currents, and also generated normal 4AP-sensitive K^+ currents predominantly mediated by $K_V1.4$ and $K_V1.5$ channels (Fig. 2). Further studies are required to address the precise mechanism for the MG53-mediated $K_V2.1$ activation in cardiomyocytes.

Materials and Methods

Physiological measurements

The test ran for 30 min or until mice failed to keep running. To examine heart functions, mice were subjected to transthoracic echocardiography and telemetric electrocardiography.[13]

Patch-clamp recordings

Ventricular cardiac myocytes were prepared and subjected to Fluo-3 Ca^{2+} measurements as described previously.[13,14] Membrane currents were recorded under the whole-cell configuration of the patch clamp technique using an Axopatch 200B patch-clamp amplifier

(Axopatch 200B, Axon Instruments). Pipette resistance was 3–5 MΩ when filled with pipette solution. The liquid junction potential between the pipette and external solution was corrected before seal formation. Series resistance was compensated and currents were filtered at 5 kHz. Step-pulse protocols and data acquisition were carried out using pCLAMP 8.0.2. software (Axon Instruments). For action potential and K^+ current recordings, the patch pipettes contained solution with the following 1.0, ATP-Mg 5.0, HEPES composition (in mM): KCl 130, $MgCl_2$ 5.0, EGTA 5.0, pH 7.2 with KOH. Myocytes were submerged in the external solution containing NaCl 143, KCl 5.4, 1.8, $CaCl_2$ $MgCl_2$ 1.0, glucose 5.5, and HEPES 5.0 (pH 7.4 with NaOH). For K^+ current measurements, 1 μM nifedipine was added to the external solution. For Ca^{2+} current measurements, the patch pipette solution containing CsCl 130, 1.0, ATP-Mg 5.0, HEPES $MgCl_2$ 5.0 and EGTA 5.0 (pH 7.2 with CsOH) and the external solution 1.0, glucose containing TEA-Cl 143, CsCl 5.4, $CaCl_2$ 1.8, $MgCl_2$ 5.5 and HEPES 5.0 (pH 7.4 with CsOH) were used.

cDNA expression in cultured cells

For labeling of cell-surface $K_V2.1$, the HA-tag sequence was introduced into the mouse $K_V2.1$ cDNA at the extracellular loop between S1 and S2 transmembrane segments to yield $K_V2.1$-HA cDNA. For coexpressing $K_V2.1$ and EGFP, the $K_V2.1$-HA cDNA was cloned into pIRES2-EGFP (BD Biosciences) to yield the p$K_V2.1$-HA-EGFP plasmid. For coexpressing $K_V2.1$ and MG53, the EGFP cDNA in p$K_V2.1$-HA-EGFP was replaced with the rabbit MG53 cDNA to yield p$K_V2.1$-MG53. Essentially the same plasmid constructions were carried out for coexpression of K^+ channels and MG53. In MG53-Ring(−), the N-terminal Ring finger motif (residue numbers 29–37) was deleted. HEK293 cells were maintained in DMEM medium containing 10% fetal bovine serum, transfected with expression plasmids (lipo-fectamine, Gibco BRL), and used for physiological and biochemical analyses after ~48 hours.

$K_V2.1$ protein chemistry

Cell surface biotinylation was carried out as described previously.[15] HEK cells (10^5 cells) were labeled with biotin in the buffer (5 ml) containing 154 mM NaCl, 7.2 mM KCl, 1.8 mM $CaCl_2$, 10 mM boric acid (pH 8.8) and 0.5 mg/ml Sulfo-NHS-SS-biotin (Pierce) at 4°C for 30 min. Biotinylated cell-surface proteins were solubilized in the buffer containing 0.1% SDS, 150 mM NaCl, 1 mM EDTA, 2 μg/ml leupeptin, 0.5 mM PMSF and 2 μg/ml antipain and 10 mM Tris-HCl (pH 7.5). After the removal of cell debris by centrifugation (30 min at 15,000 ×g), the resulting supernatant was reacted with streptavidin-conjugated resin (Pierce) overnight at 4°C with agitation. After washing the resin, biotinylated proteins were eluted from the resin using a sampling buffer for SDS-polyacrylamide gel electrophoresis at 90°C for 5 min, and analyzed by western blotting using an antibody to $K_V2.1$ (Upstate). The density of immunoreactivity was digitalized and analyzed using Meta Imaging software (Molecular Devices).

$K_V2.1$ dynamics in cultured cells

To monitor intracellular trafficking of $K_V2.1$, HEK cells cultured in glass-bottom dishes (Mat Tek) were transfected with the plasmids described above, and HA-tagged $K_V2.1$ expressed on the cell surface was labeled with anti-HA antibody (Roche) conjugated with CypHer 5E (Amersham Biosciences) at 37°C for 30 min. CypHer 5E fluorescence images (excitation at 543 nm and emission at >610 nm) were captured at 4 frames/min using a confocal microscope (FV300, Olympus) at 34°C. To examine the internalization of HA-tagged $K_V2.1$ on the cell membrane, cells were incubated with the antibody complex labeled with Cypher 5E at 4°C for 30 min. Then, cells were quickly incubated at 34°C. Fluorescence images (excitation at 640 nm and emission at >690 nm) were captured at 2 frames/min using a CCD camera (ORCA-ER, Hamamatsu Photonics, Japan) mounted on a microscope

equipped with a polychrometor, and analyzed with Meta Fluor software (Molecular Devices).

Supplementary Material

Refer to Web version on PubMed Central for supplementary material.

Acknowledgments

We thank Ms. Miyuki Kameyama for her expert assistance, Dr. Takashi Nagasawa for testing serum amino acids, and Drs. Sigeru Yokoyama and Haruhiro Higashida (Kanazawa University) for providing us with the K_V1.2 and K_V3.1 cDNAs. This work was supported in part by grants from the Ministry of Education, Culture, Sports, Science and Technology of Japan, the Ministry of Health and Welfare of Japan, the National Institute of Health of the USA, the Ono Medical Research Foundation and the Japan Foundation for Applied Enzymology.

References

1. Reymond A, Meroni G, Fantozzi A, Merla G, Cairo S, Luzi L, et al. The tripartite motif family identifies cell compartments. EMBO J 2001;20:2140–51. [PubMed: 11331580]
2. Short KM, Cox TC. Subclassification of RBCC/TRIM superfamily reveals a novel motif necessary for microtubule binding. J Biol Chem 2006;281:8970–80. [PubMed: 16434393]
3. Ozato K, Shin D-M, Chang T-H, Morse HC III. TRIM family proteins and their emerging roles in innate immunity. Nat Rev Immunol 2008;8:849–60. [PubMed: 18836477]
4. Weisleder N, Takeshima H, Ma J. Immuno-proteomic approach to excitation-contraction coupling in skeletal and cardiac muscle: molecular insights revealed by the mitsugumins. Cell Calcium 2008;43:1–8. [PubMed: 18061662]
5. Cai C, Masumiya H, Weisleder N, Matsuda N, Nishi M, Hwang M, et al. MG53 nucleates assembly of cell membrane repair machinery. Nat Cell Biol 2009;11:56–64. [PubMed: 19043407]
6. Cai C, Masumiya H, Weisleder N, Pan Z, Nishi M, Ko J-K, Komazaki S, Takeshima H, Ma J. MG53 regulates membrane budding and exocytosis in muscle cells. J Biol Chem 2009;284:3314–22. [PubMed: 19029292]
7. Nerbonne JM, Nichols CG, Schwarz TL, Escande D. Genetic manipulation of cardiac K^+ channel function in mice. What have we learned, and where do we go from here? Circ Res 2001;89:944–56. [PubMed: 11717150]
8. Adie EJ, Kalinka S, Smith L, Francis MJ, Marenghi A, Cooper ME, et al. A pH-sensitive fluor, CypHer 5, used to monitor agonist-induced G protein-coupled receptor internalization in live cells. Biotechniques 2002;33:1156–7.
9. Misonou H, Mohapatra DP, Park EW, Leung V, Zhen D, Misonou K, et al. Regulation of ion channel localization and phosphorylation by neuronal activity. Nat Neurosci 2004;7:711–8. [PubMed: 15195093]
10. Martens JR, Sakamoto N, Sullivan SA, Grobaski TD, Tamkun MM. Isoform-specific localization of voltage-gated K^+ channels to distinct lipid raft populations. Tageting of K_V1.5 to caveolae. J Biol Chem 2001;276:8409–14. [PubMed: 11115511]
11. Maguy A, Hebert TE, Nattel S. Involvement of lipid rafts and caveolae in cardiac ion channel function. Cardiovasc Res 2006;69:798–807. [PubMed: 16405931]
12. Martens JR, Navarro-Polanco R, Coppock EA, Nishiyama A, Parshley L, Grobaski TD, et al. Differential targeting of Shaker-like potassium channels to lipid rafts. J Biol Chem 2000;275:7443–6. [PubMed: 10713042]
13. Yoshida M, Minamisawa S, Shimura M, Komazaki S, Kume H, Zhang M, et al. Impaired Ca^{2+} store functions in skeletal and cardiac muscle cells from sarcalumenin-deficient mice. J Biol Chem 2005;280:3500–6. [PubMed: 15569689]
14. Ito K, Yan X, Tajima M, Su Z, Barry WH, Lorell BH. Contractile reserve and intracellular calcium regulation in mouse myocytes from normal and hypertrophied failing hearts. Circ Res 2000;87:588–95. [PubMed: 11009564]

15. Leung YM, Kang Y, Xia F, Sheu L, Gao X, Xie H, et al. Open form of syntaxin-1A is a more potent inhibitor than wild-type synataxin-1A of K_V2.1 channels. Biochem J 2005;387:195–202. [PubMed: 15518587]

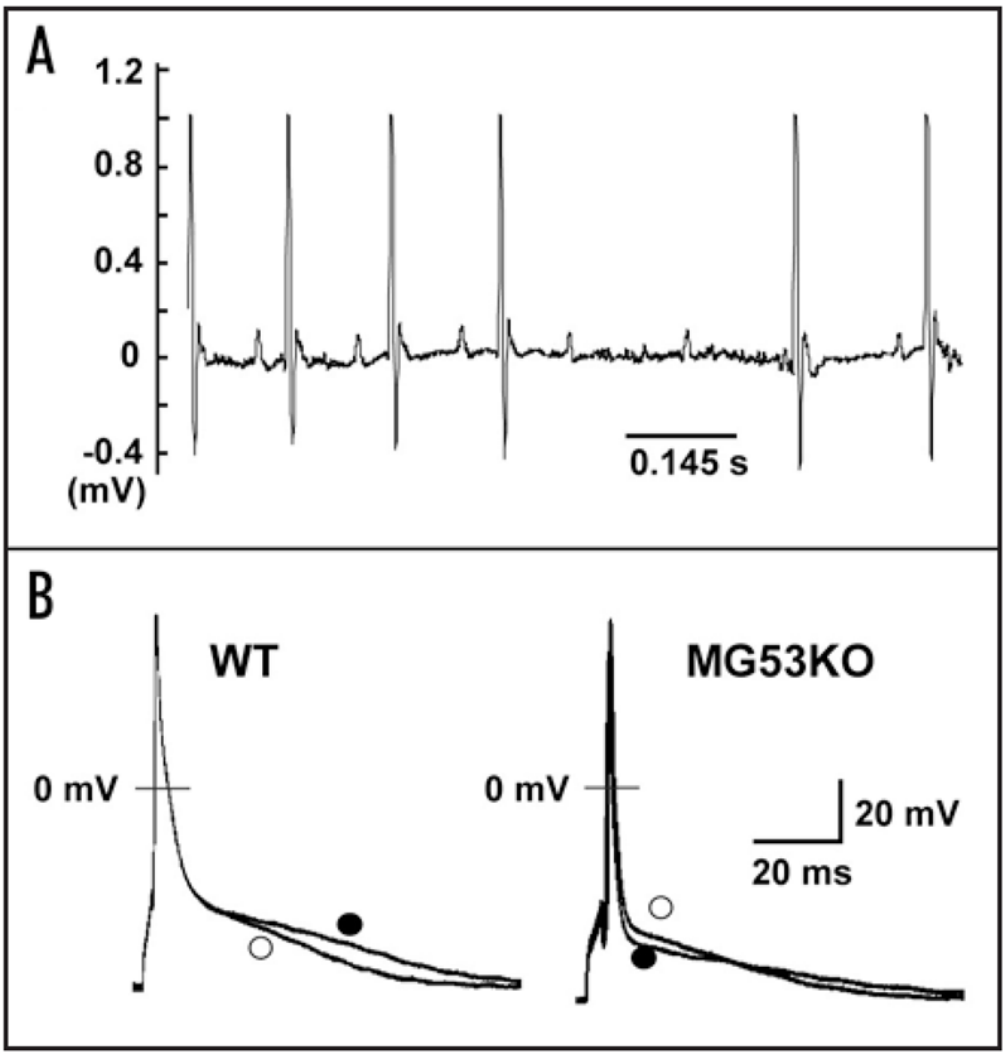

Figure 1.

Abnormal physiological features in MG53-knockout heart. Complete atrioventricular block detected in MG53-knockout mice (A). The event was recorded in MG53-knockout mice injected with atropine (0.5 μg/ kg i.p.). A similar event was also detected under basal conditions in MG53-knockout mice (n = 3 from 9 mice), but not in wild-type mice (n = 9 mice). Irregular action potential configuration in MG53-knockout cardiac myocytes (B). Representative traces from amphotericin B-perforated patch recordings in the absence (open circle) and presence (closed circle) of 1 μM isoproterenol. The data from statistical analysis are summarized in Table 1.

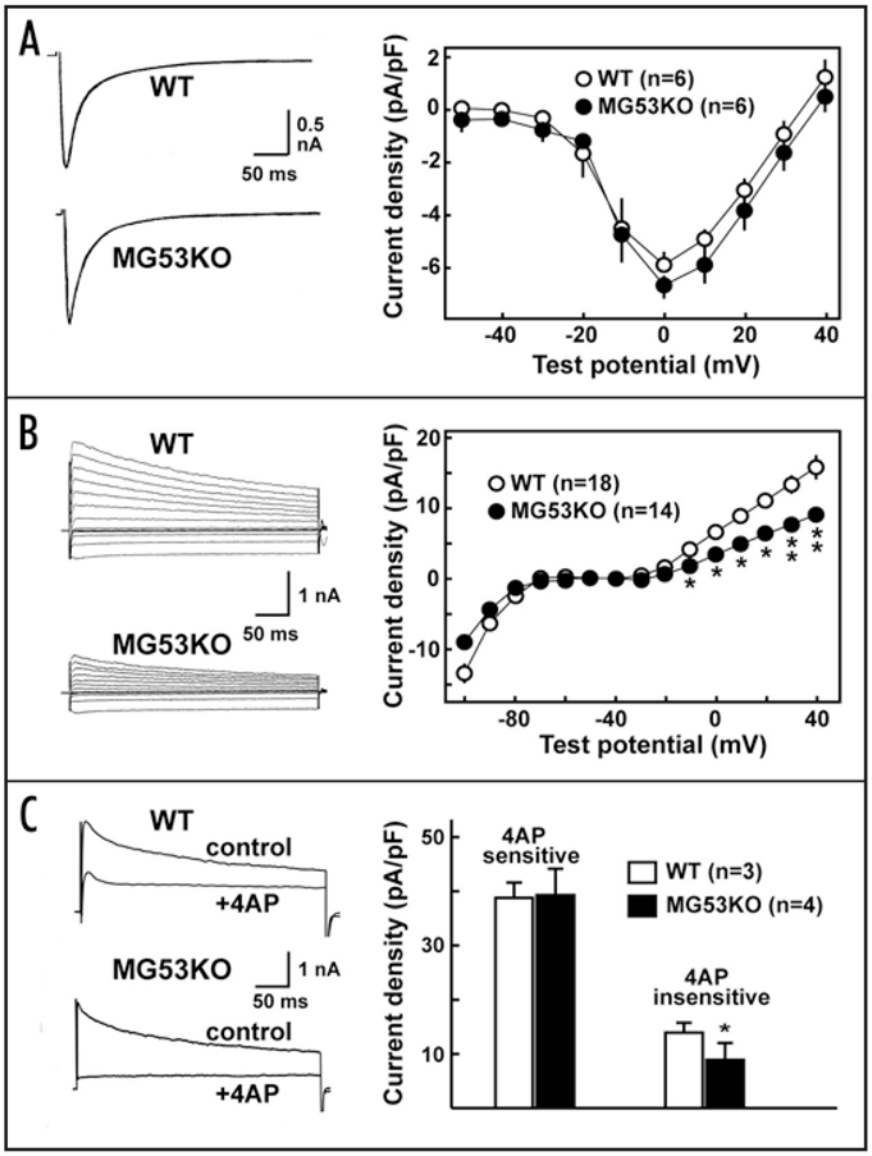

Figure 2.

Impaired delayed rectifier K^+ currents in MG53-knockout cardiomyocytes. Recording of L-type Ca^{2+} channel activity (A). Typical Ca^{2+} current traces and current-voltage relationships are shown. No significant differences were detected in the L-type Ca^{2+} channel activity between the genotypes. Recording of voltage-gated K^+ channel activity (B). Typical K^+ current traces and current-voltage relationships are shown. Reduced current densities were observed at higher test potentials in MG53-knockout myocytes. Measurement of transient outward K^+ currents (C). Typical K^+ current traces in the presence and absence of 4AP (50 μM) at the test potential of +40 mV, and the statistical comparison of current densities are shown. A significantly reduced 4AP-insensitive current density was observed. The data represent mean ± SEM. and significant differences between the values from wild-type and MG53-knockout myocytes are indicated by asterisks (*$p < 0.05$ and **$p < 0.01$ in t-test).

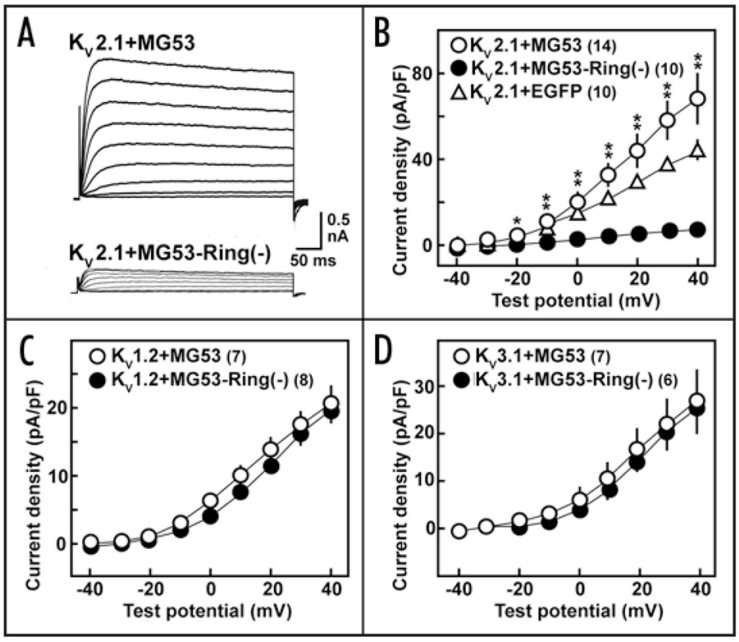

Figure 3.

Facilitation of K_V2.1 currents by MG53 in HEK cells. Representative K^+ current traces in HEK cells transfected with K_V2.1-MG53 and K_V2.1-MG53-Ring(−) cDNAs (A). Effects of MG53 and MG53-Ring(−) on voltage-gat-ed K^+ current densities by K_V2.1 (B), K_V1.2 (C) and K_V3.1 (D). The recorded data are summarized in the current-voltage relationships. The results for cells transfected with K_V2.1-EGFP cDNA are also shown in B. The numbers of cells examined are shown in parentheses. The data represent mean ± SEM and significant differences between MG53 and MG53-Ring(−) are indicated by asterisks (*$p < 0.05$ and **$p < 0.01$ in t-test).

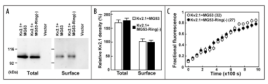

Figure 4.

No effect of MG53 on $K_V2.1$ protein density and internalization in HEK cells. Immunoblot analysis of $K_V2.1$ in HEK cells transfected with $K_V2.1$-MG53 and $K_V2.1$-MG53-Ring(−) cDNAs. Immunoreactivities for total cellular $K_V2.1$ proteins and biotinylated cell-surface $K_V2.1$ proteins were analyzed (A), and no significant difference was observed between the groups (B). Monitoring of $K_V2.1$ internalization into acidic vesicles (C). After labeling cell-surface HA-tagged $K_V2.1$ with CypHer 5E at cold temperature, warmed HEK cells were subjected to imaging analysis using a fluorescence microscope mounted with a CCD camera. Increasing fluorescence was normalized with the maximum value of individual cell recorded. No essential difference in the slope of increasing fluorescence was observed between the groups.

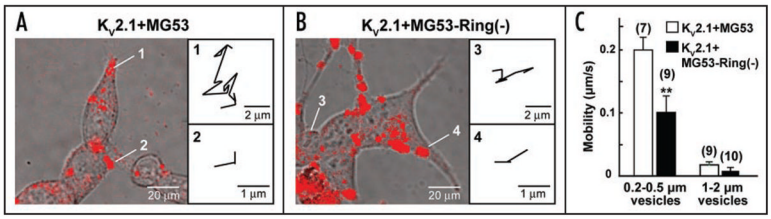

Figure 5.

Mobility of K_V2.1-containing vesicles is facilitated by MG53 in HEK cells. Dynamics of K_V2.1-containing acidic vesicles in cells coexpressing MG53 (A) and MG53-Ring(−) (B). After sufficiently labeling cell-surface HA-tagged K_V2.1 with CypHer 5E, HEK cells were subjected to imaging analysis using a confocal microscope. Typical trajectories (150 s duration) of fluorescent vesicles containing K_V2.1 in cells expressing MG53 or MG53-Ring(−) are shown; analyzed vesicles are numbered in the confocal images (see supplementary movies for details). Comparison of vesicular mobility between cells expressing MG53 and MG53-Ring(−) (C). The data represent mean ± SEM and significant differences between cells expressing MG53 and MG53-Ring(−) are indicated by asterisks (**$p < 0.01$ in t-test).

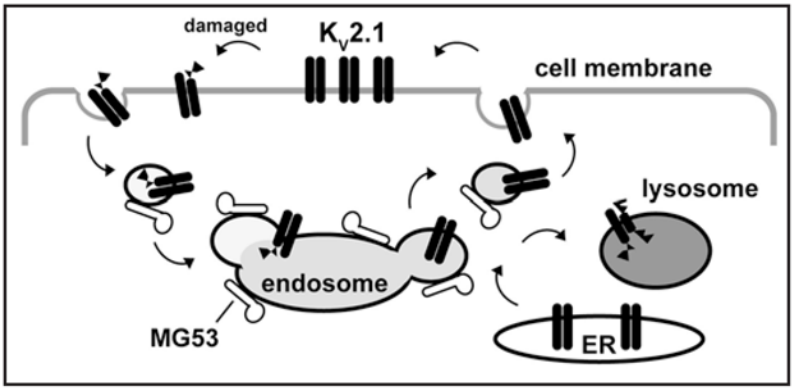

Figure 6.

Proposed function of MG53 for $K_V2.1$ maintenance in cardiomyocytes. Previous studies have established that MG53 has a vital role in vesicular trafficking for membrane repair and budding in muscle cells. Present data suggest that MG53 facilitates $K_V2.1$ currents by increasing its active population on the cell membrane in cardiomyocytes, and also that $K_V2.1$ undertakes migrations between the cell membrane and endosome-like vesicles. This migration cycle may tightly link with the quality control of cell-surface $K_V2.1$ channels; in other words, MG53 activates trafficking of endosome-like vesicles and likely stimulates the clearance of inactivated $K_V2.1$ proteins from the cell membrane. Therefore, it is reasonable that during MG53-mediated endosomal trafficking, active and damaged channel proteins may be sorted into the recycling endosome and lysosome/proteosome, respectively. The loss of MG53 may impair the efficacy of this quality control to elevate inactive population of $K_V2.1$ to the cell membrane in cardiomyocytes.

Table 1

Action potential in MG53-knockout ventricular myocytes

	Control		Isoproterenol (1 μM)	
	Wild type (4)	**MG53KO (4)**	**Wild type (4)**	**MG53KO (4)**
RP (mV)	−71.1 ± 1.8	−69.0 ± 4.5	−70.4 ± 2.3	−67.6 ± 4.6
OS (mV)	52.3 ± 4.3	43.4 ± 2.5*	47.6 ± 5.1	40.1 ± 2.2*
Amplitude (mV)	123.0 ± 4.6	112.4 ± 2.0*	118.0 ± 5.4	107.8 ± 5.0
APD20 (ms)	5.66 ± 1.90	5.24 ± 1.72	4.94 ± 2.23	5.92 ± 2.49
APD50 (ms)	11.9 ± 2.7	7.23 ± 2.43	11.0 ± 6.6	7.32 ± 3.08
APD90 (ms)	74.1 ± 7.3	42.4 ± 7.7*	95.4 ± 19.1	42.2 ± 11.8*
APD95 (ms)	95.1 ± 14.0	65.2 ± 4.9*	125.8 ± 23.5	74.6 ± 6.9*

Recordings were carried out by current clamp with the amphoterisin B-perforated patch technique. RP, resting potential; OS, overshoot potential; Amplitude, action potential amplitude; APD20-95, action potential duration at 20–95% of repolarization. Data indicate mean ± SEM.

* ($p < 0.05$ in t-test between the genotypes) and n values are shown in parentheses.

Table 2

Contraction and Ca^{2+} transient in MG53-knockout ventricular myocytes

	Control		Isoproterenol (1 μM)	
	Wild type (17)	**MG53KO (13)**	**Wild type (5)**	**MG53KO (10)**
Myocyte length (μm)	112 ± 4	111 ± 3	110 ± 2	107 ± 4
Fractional shortening (%)	7.5 ± 0.6	7.5 ± 0.7	13.1 ± 1.1	9.3 ± 0.9*
Time to 50% relaxation (ms)	39 ± 3	40 ± 3	35 ± 2	41 ± 5
Peak systolic $[Ca^{2+}]_i$ (nM)	532 ± 40	569 ± 29	912 ± 48	626 ± 38**
End diastolic $[Ca^{2+}]_i$ (nM)	82 ± 5	72 ± 5	80 ± 3	78 ± 5
Time to 50% decline (ms)	45 ± 3	55 ± 4	32 ± 2	41 ± 4

Single cardiomyocytes were examined in the bathing solution containing 1.5 mM $CaCl_2$ at 35–36°C. Data indicate mean ± SEM.

* $p < 0.05$ and

** $p < 0.01$ in t-test between the genotypes and n values are shown in parentheses.